On Ordering of Functional Groups by Confining Grafted Chains, Star Polymers, or Polymer-Stabilized Nanoparticles

Maziar Heidari, Matthieu Labousse, Ludwik Leibler

On ordering of functional groups by confining grafted chains, star polymers or polymer-stabilized nano-particles

Maziar Heidari, Matthieu Labousse,* and Ludwik Leibler*

Gulliver, CNRS UMR 7083, ESPCI Paris and PSL University, 75005 Paris, France.

E-mail: matthieu.labousse@espci.fr; Ludwik.Leibler@espci.fr

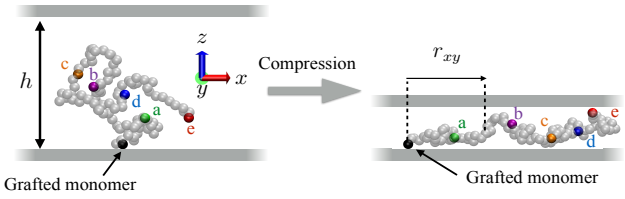

Abstract

Understanding and controlling the self-organization of functionalized sites are crucial in biological systems, in catalysis, and to target drug delivery. Here we investigate the possibility of spatiotemporal self-organization offered by the development of sequence-controlled polymers. As a key factor in reducing the configurational entropy of a chain, confinement can enhance or hinder the ordering of chain segments. Using molecular dynamics simulations and scaling concepts, we show that the segments of a closely grafted chains inside a patch are radially localized under planar confinement. We investigate the statistical properties of this self-organization and show that it results from an interplay between confinement and excluded volume between monomers. Increasing

the length of polymers as well as the number of chains inside the patch enhances the localization and spatial sequencing order of the segments.

Introduction

Today polymer chemistry enables synthesis of chains in which functional groups are inserted in a controlled precise position in a macromolecular chain.[1–8] The question arises how to transform this primary structure into an organized sequence in space. Indeed many biological and chemical processes involve temporal and spatial ordering of functionalized groups. For example, cell membrane fusion requires sequential rearrangement of ligands and receptors of transmembrane proteins.[9] In vesicle fusion during synaptic neurotransmission, the activity of SNARE proteins relies on spatial ordering of functional groups.[10] In the self-healing process, the organization and ordering of the functionalized sites of supramolecular polymers play a critical role at the rupture.[11] In the catalytic activity and enzymatic regulation of many biological mechanisms, the activity severely depends on the sequencing and cooperativity between functionalized sites along the molecules.[1,12] In many cases, these processes involve specific enthalpic interactions or superselective strategies.[13,14]

A cooperation between functionalized sites should satisfy two conflicting constraints (i) be accessible in a relatively confined region of space but (ii) reachable in a given order. In the absence of any of the aforementioned mechanisms where entropy and excluded volume interactions only remain, these two constraints seem hard to reconcile. In that context, attaching functionalized sites along a grafted polymer chain is a strategy to localize many active sites in a relatively confined region of space. However, without any designed enthalpic interactions within the chain, the number of chain conformations is tremendous so that it remains unclear why these multiple sites spatially order. In this article we propose a novel strategy to achieve this goal by confining a polymer chain.

A polymer chain of size N confined below its gyration radius, say by two parallel walls at

a distance h, behaves as an effective chain of *blobs*.[15,16] The blob size saturates the monomer position fluctuations correlation functions normal to the walls so that the macroscopic properties resulting from the chain entropy are strongly impacted. The chains are laterally stretched. The stretching also occurs for ring polymers and stiff chains .[17–19] It has also been shown that ungrafted ring polymers confined between two parrallel walls exhibit a spatial structure.[20] There have been different theoretical and numerical investigations about grafted chains and star polymers under confinement.[21–26] Scaling laws for a confined chain indicate that the position fluctuations parallel to the confining wall evolve as $\langle r_{xy}^2 \rangle^{1/2} \sim (N^3/h)^{1/4}$. The reduction of the free energy scales as $N/h^{5/3}$ and is much more pronounced than a logarithmic law expected from a simple concentration effect under confinement. This suggests that the cooperativity originating from excluded volume between monomer plays a critical role. Here, by using molecular dynamics simulations and scaling arguments, we show that this cooperativity can be leveraged to order chain segments. We evidence a fundamental self-organization mechanism which has not been elucidated so far.

We start by defining our numerical methods. Then we show that under confinement the functionalized sites positioned along a grafted polymer spatially ordered. We analyze the mean position and position fluctuations for single chain and multichain configurations and rationalize their behavior. Then we show that the azimuthal fluctuations play a critical role in the ordering of multichain configuration. Finally, we analyze the efficiency of spatial sequencing of the chain's segments that rises up when a large number of chains are closely grafted in a patch and then conclude.

Numerical methods

We use molecular dynamics (MD) to simulate a grafted linear polymer chain under confinement. A coarse-grained model of polymer chain known as Kremer-Grest model is employed to account for the interactions between the chain's monomers.[27] We consider a polymer chain of

length $N = 100$ unless otherwise stated. Simulation cases with longer chain length $N = 500$ are also studied. A monomer j ($j = 1, \ldots, N$) is identified with its dimensionless monomer index n_j/N. The total potential (U) consists of non-bonded and bonded interactions, a constraining potential and confining repulsive walls: $\mathrm{U} = \mathrm{U_{LJ}} + \mathrm{U_{FENE}} + \mathrm{U_C} + \mathrm{U_W}$. The interaction between the monomers of the chain is given by a Lennard-Jones (LJ) potential

$$\mathrm{U_{LJ}} = 4 \sum_{i,j,r_{i,j}<R_{ij}} \epsilon_{ij} \left[\left(\frac{a}{r_{i,j}} \right)^{12} - \left(\frac{a}{r_{i,j}} \right)^{6} \right], \tag{1}$$

where $r_{i,j}$ is the distance between the monomers i and j, and a is the length scale of the LJ potential. For the neighboring monomers along the chain $\epsilon_{ij} = \epsilon_{rep}$ and the cut-off radius is $R_{ij} = 2^{1/6}a$ while for non-bonded pairs, $\epsilon_{ij} = \epsilon$ and $R_{ij} = 3a$. The maximum distance between bonded (neighboring) pairs is controlled by FENE potential,[27]

$$\mathrm{U_{FENE}} = \frac{k_s R_0^2}{2} \sum_{<i,j>} \ln \left[1 - \left(\frac{r_{i,j}}{R_0} \right)^2 \right]. \tag{2}$$

Where k_s and R_0 are the stiffness and the maximum stretching limit of the bonds. We choose the LJ length scale (a) as the length unit and the thermal energy (k_BT) as the energy unit, where k_B is the Boltzmann constant and T is the system temperature. The mass of all monomers m is identical and the characteristic time scale is set as $\tau = \sqrt{ma^2/k_BT}$. The simulations are carried out by LAMMPS program in canonical ensemble (NVT) using the Langevin thermostat.[28,29] In all simulations, we set the parameters $\epsilon_{rep} = k_BT$, $k_s = 30k_BT$ and $R_0 = 1.5a$. The strength of the cohesive interaction between the monomers is set by $\epsilon = 0.1k_BT$ so as to sample the chain's conformations in good solvent. The time step and damping parameter for Langevin thermostat are chosen, respectively to be $\Delta t = 0.01\tau$ and $\lambda = 10\tau$. One end of the chain is fixed by harmonic potential with a spring constant $k_c = 10^3 k_BT/a^2$:

$$\mathrm{U_C} = \frac{k_c}{2} \|\mathbf{x}^1 - \mathbf{x}_0^1\|^2. \tag{3}$$

The first monomer of each chain is fixed at the position $\mathbf{x}_0^1 = [0, 0, 0]$. As shown by thick gray lines in Figure 1, two repulsive harmonic potentials are used to confine the monomers of the chain within the height interval [0, h],

$$\mathrm{U}_{\mathrm{W}}^{L,U} = k_{\mathrm{w}} \sum_i \left(H_i^{L,U} - r_c \right)^2, \quad H_i^{L,U} < r_c, \tag{4}$$

where $H_i^L = z_i + r_c$ and $H_i^U = h + r_c - z_i$ for the lower and upper wall, respectively, and z_i is the z-component of position of the i^{th} monomer. We used $k_{\mathrm{w}} = 10^3 k_B T/a^2$ and $r_c = 2a$ in all simulations which leads to equal average penetration length in both upper and lower walls $\langle z_{pe}^{L,U} \rangle \approx 0.02a$ which is also verified by the Boltzmann weighted average $\langle z_{pe}^{L,U} \rangle = \int dz\ z \exp\left(-\beta U_W^{L,U}\right) / \int dz \exp\left(-\beta U_W^{L,U}\right)$. We graft chains on a single square lattice patch with constant separation distance $l_d = 2a$. We call functionality f the number of grafted chains inside the patch. During the first $10^4\tau$ simulation time steps, the grafted chains is equilibrated in free state; i.e., the upper wall is far beyond the gyration radius of the chain ($h \gg R_g$). Then the upper wall is lowered slowly (confining rate $10^{-5}a/\tau$) until it reaches the target confining level. The total production run is set $12 \times 10^6\tau$ with sampling time interval 10τ. Thus, the total simulation run is remarkably larger than the slowest relaxation time obtained from Rouse model, $\tau_p = \zeta N^2 a^2 / 3\pi^2 k_B T$,[30–33] given the chain length $N = 100$ and the friction coefficient of solvent is $\zeta = 10^{-1} m/\tau$. This coefficient is obtained from the ratio of the monomer mass to the damping coefficient used in Langevin thermostat, i.e. m/λ[29,34] the slowest relaxation time becomes $\tau_p \approx 34\tau$. Additionaly, we have calculated the relaxation time of end-to-end distance using characteristic time of its autocorrelation function for the grafted chain, $\phi(t) = \langle R_{ee}(t) R_{ee}(0) \rangle - \langle R_{ee} \rangle^2 / [\langle R_{ee}^2 \rangle - \langle R_{ee} \rangle^2]$. For the long time limit ($t \to \infty$), the correlation decays exponentially, $\phi(t) \propto \exp(-t/\tau_r)$.[35] We obtain $\tau_r = 144\tau$ for the chain of length $N = 100$. The relaxation time obtained from the correlation function of R_{ee} is larger than the Rouse relation time due to the excluded volume effect; however, it is still much shorter than the total simulation time. To perform statistics,

the total time steps is divided into four blocks of equal size, and we report the average and standard errors of the mean corresponding to the four blocks as the error bars. The simulation box is cubic with side L which is set, unless otherwise stated, larger than the twice of chain's contour length ($L > 2Na$), and the periodic boundary conditions are set along x and y directions. Thus, for the isolated grafted chain or patch, the system does not interact with periodic images. The equilibrium probability density of each functionalized sites (fs) position can be calculated along radial and perpendicular directions through discretization of space with circular elements. The mean radius and thickness of the elements are r_{xy} and Δr, respectively. The following expression describes the probability density function of the i^{th} fs:

$$
\begin{aligned}
p_i(r_{xy}) 2\pi r_{xy} \Delta r &= \frac{\sum_k \int_0^h dz \delta\left(z - z^{i,k}\right) \delta\left(r_{xy} - r_{xy}^{i,k}\right)}{M}, \\
p_i(z) \Delta z &= \frac{\sum_k \int_0^\infty dr_{xy} \delta\left(z - z^{i,k}\right) \delta\left(r_{xy} - r_{xy}^{i,k}\right)}{M} \\
M &= \sum_k \int_0^h \int_0^\infty dz dr_{xy} \delta\left(z - z^{i,k}\right) \delta\left(r_{xy} - r_{xy}^{i,k}\right). \qquad (5)
\end{aligned}
$$

Here, $r_{xy}^{i,k}$ and $z^{i,k}$ are respectively, the radial and normal positions of the i^{th} fs at time t_k. Where $\Delta r = a$ and $\Delta z = 0.5a$ are the size of the element. The function $\delta(x)$ is 1 when $|x| < \Delta x$ and otherwise 0. The sum runs over M time steps of each simulation block as explained earlier.

Results

Figure 1 shows two typical numerical instantaneous snapshots of the polymer in unconfined and confined situation. The first monomer is grafted onto the lower interface. We divide the contour length of each chain into five uniform segments and label sequentially the last monomer of each segments $\{a, b, c, d, e\}$. We call these tagged monomers "*functionalized sites*

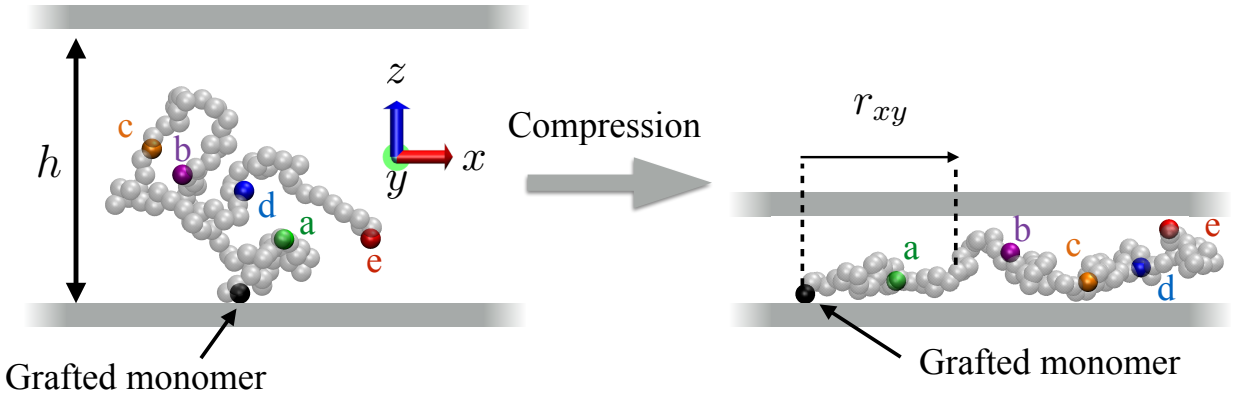

Figure 1: Snapshots of a single grafted chain system under confinement. The chain has $N = 100$ monomers and five equally spaced monomers which are named functional sites (*fs*), indexed with $\{a, b, c, d, e\}$ and marked with different colors. The grafted monomer is shown in black. The confining walls are shown in thick gray lines. The distance between each *fs* and the grafting position in the $x - y$ plane is denoted by r_{xy}. The system is visualized by using the package VMD.[36]

(*fs*)" although there is no difference between the interaction of *fs* and the rest of monomers. When the confinement length h is smaller than the chain gyration radius, we observe numerically that the *fs* spatially rearrange and find new positions exhibiting a sequential order. The objectives of this article is to rationalize the statistical robustness of this phenomenon upon different confinement ratios for single-chain and multichain configurations.

Ordering by Confining

The chain is embedded within a thermal bath so the positions of the *fs* changes dynamically. We investigate in Figure 2a and 2b the probability density of finding a given *fs* at given dimensionless radius $r_{xy}/R_{ee} = 0.32$ where R_{ee} denotes the chain end-to-end distance. For a single free chain of size $N = 100$, i.e. when the chain is neither grafted nor confined, the end-to-end distance is $R_{ee} = 15.7a$. This value grows to $R_{ee} = 39.7a$ for the chain of size $N = 500$. In the unconfined state $h/R_{ee} = 3$, the maximum of likelihood is vertically aligned with the grafted position ($r_{xy} = 0$) for all *fs* as expected from the axisymmetry of the system. In contrast, in the confined state, the *fs* are depleted from the center and

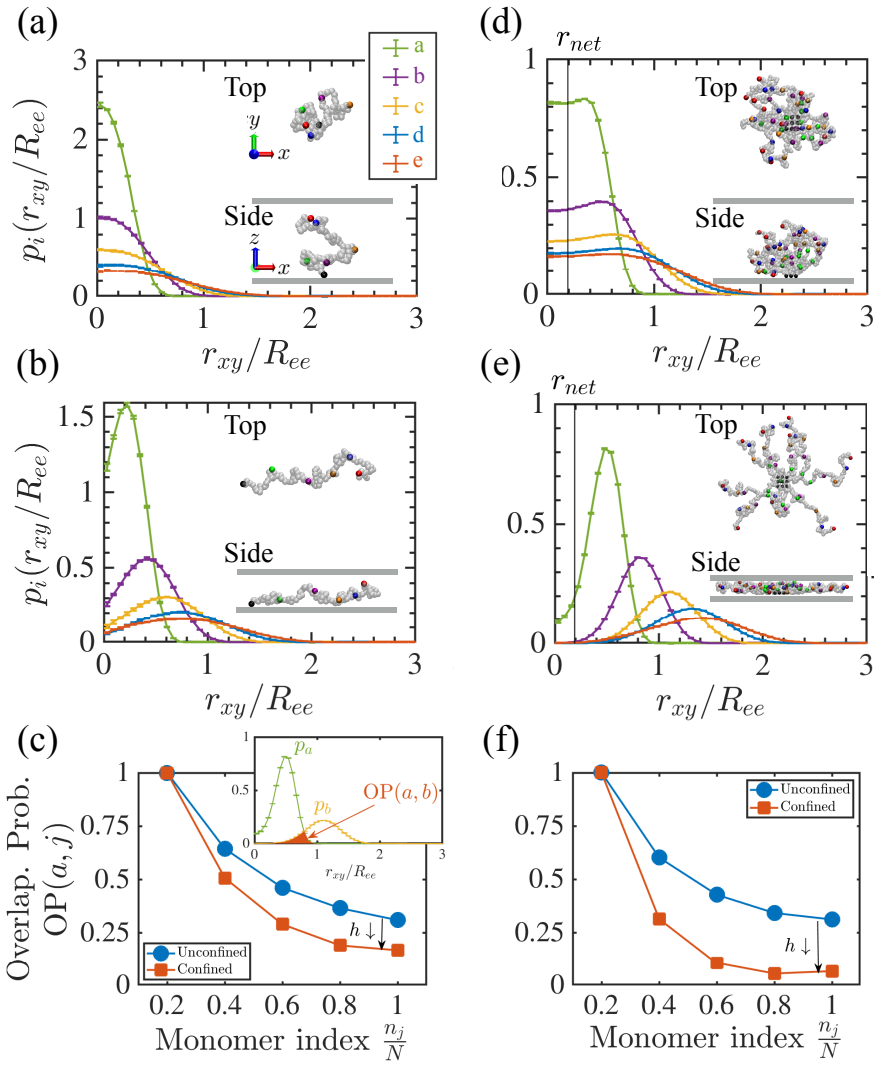

Figure 2: Emergence of radial ordering under confinement. (a)-(b) (respectively (d)-(e)) Radial probability distribution of the (fs) radial positions for one single chain (respectively for a 3×3 patch). The colors stand for tagged monomers. The inset represents snapshots from top and side views. The first row panels represent unconfined states, $h/R_{ee} = 3$ while the second row panels correspond to a confined state $h/R_{ee} = 0.37$. (c) (respectively (f)) The overlapping probability (OP) between two fs as shown in the inset of panel for a single chain (respectively for a 3×3 patch). Especially the tagged monomers $a, \ldots, e$ correspond to normalized monomer indices $n_j/N = 0.2, \ldots 1$.

the location of the maxima of likelihood of the *fs* separate and shift towards larger radii. We note that in confined situations $h/R_{ee} \lessapprox 1$ the position of the maximum of likelihood becomes dependent on the level of confinement (See Figure 2a in SI). For the $h/R_{ee} < 1$, the vertical probability density of *fs*, $p_i(z)$, is symmetric with respect to the middle of slit with a maximum likelihood at $h/2$ (see Figure 2b of SI). In this regime, the vertical position fluctuations are equal to the confining level. The efficiency of the ordering can be assessed by measuring first the Overlapping Probability (OP) between two tagged monomers, say $i =$\{a\},...,\{e\} and $j =$\{a\},...,\{e\}. We define it (see inset of Figure 2c) as

$$\mathrm{OP}(i,j) = 2\pi \int_0^\infty dr_{xy} r_{xy} \min\left(p_i(r_{xy}), p_j(r_{xy})\right). \tag{6}$$

Thus, the value of OP is one when the probability of two *fs* overlap exactly, and it becomes zero when the two are completely localized and separated. The OPs between the *fs* $\{a\}$ and the others are shown in Figure 2c. The OPs monotonically decrease for unconfined and confined states but in a quantitatively different manner: the confinement enhances the radial localization up to 53 %. The ordering of functional sites can also be explained by using the intrinsic shape anisotropy of random walk in space due to the entropic effect.[37–39] In this picture, the instantaneous extended trajectory of self-avoiding random walk can be approximated by an prolate ellipsoid whose axes have ensemble-average aspect ratios 14.8:3.06:1 along the moments of the radius of gyration.[39,40] The free ellipsoid in space can orient randomly; however, planar confinement can reduce its orientation entropy and consequently order steps along the trajectory (see Figure 3 of SI). We shall see below that the remaining azimuthal degree of freedom limits the ordering. To improve drastically the efficiency of ordering, we consider a system made of f chains grafted and grouped on a square $n \times n$ patch with separation $2a$. A snapshot of the 3×3 ($f = 9$) patch of grafted chains is shown in the inset of Figure 2d. Analogously, the probability density of *fs* in Figure 2d

of an unconfined patch of size $f = 9$ has a similar decrease as in the single chain but with a more pronounced depletion zone at the center due to the excluded volume of the other grafted chains. The results of other patches are shown in Figure S7 and S8. The half size of the region on which the monomers are grafted is indicated with $r_{net} = \sqrt{f}a$ (see Figures 2d and e). Under confinement, Figure 2e shows that the density probabilities of finding the *fs* at a given radius r_{xy} sharpen while their maximum of likelihood separate. We estimate the efficiency of this spatial separation by computing the Overlapping Probability between the *fs* {a} and *fs* j ={a},...,{e}. For both unconfined and confined situation, Figure 2f shows that the OPs decrease monotonically. The unconfined state of a patch of chains (Fig. 2f) hardly differs from that of a single-chain case (Fig. 2c). However, and in contrast with a single chain case, the OPs of patched chains under confinement sharply decrease meaning that the efficiency of ordering of the *fs* is improved. It is noteworthy that the OP of the confined patch is nonmonotonic. This can be explained by the fact that the chain's end has more degrees of freedom to explore the confined space.

Evolution of Radial Fluctuations

We propose now to rationalize the origin of this ordering by measuring the mean position fluctuations of the *fs* in the confined regime. We compare our results for a single chain with the blob theory to find a scaling law for the lateral size of the confined grafted chain[32,39,41,42] and use then Self-Avoiding Walk (SAW) theory to rationalize our data. Under confinement of size h, the chain is renormalized into a linear string of blobs of size h. The number of monomers inside each blob is $g = (h/a)^{1/\nu}$, where $\nu = 3/5$ is the Flory exponent for a three-dimensional chain in a good solvent. We investigate in Figure 3a (respectively 3b) the evolution of mean position $\langle r^i_{xy} \rangle$ (resp. position fluctuations $\chi^i_{xy} = \langle \left(r^i_{xy}\right)^2 \rangle - \langle r^i_{xy} \rangle^2$) of the *fs* with their normalized index within the chain n_j/g. We consider two different chain lengths $N = 100$ and 500 for the same level of confinement. The mean position increases with the monomer index with a power law $\left\langle r^i_{xy} \right\rangle \sim h(n_i/g)^{3/4}$. This behavior can be predicted by

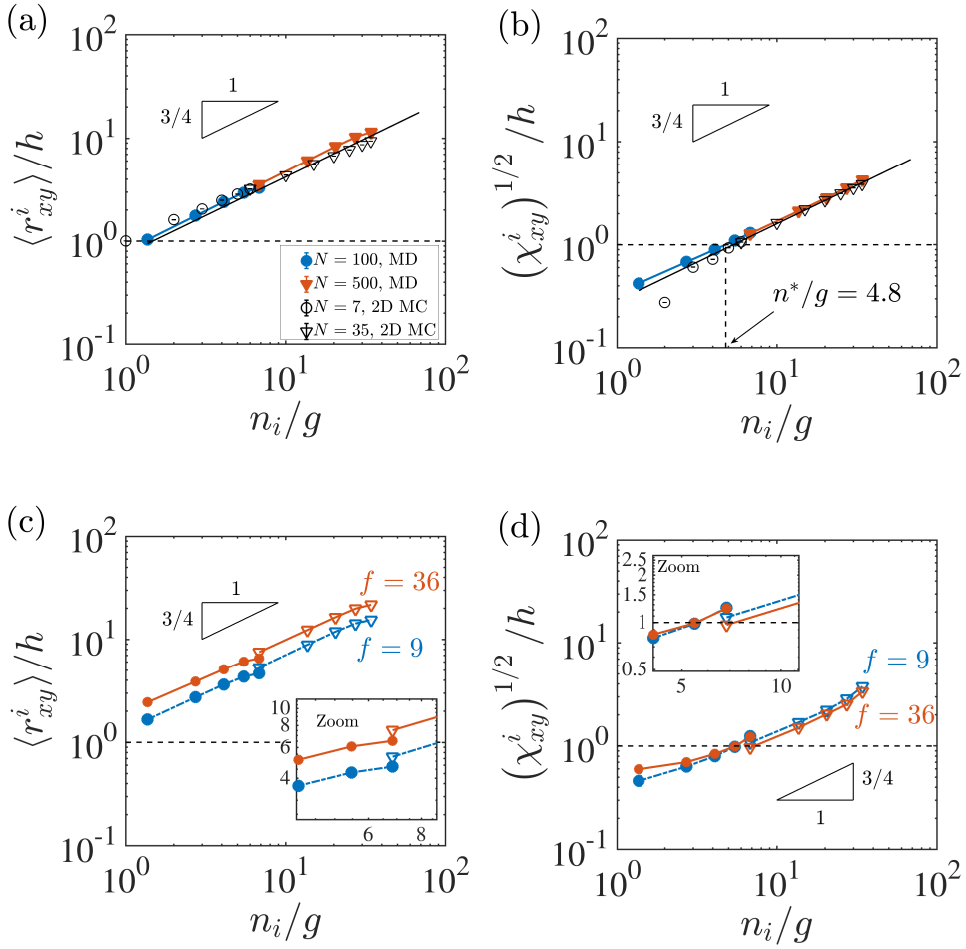

Figure 3: Average radial position ($\langle r^i_{xy}\rangle/h$) and fluctuations of *fs* (χ^i_{xy}/h) as a function of monomer index of that *fs* normalized by the blob size n_i/g. The results of a single chain are shown in (a) and (b) while the results of the patches of grafted chain with $f = 9$ and $f = 36$ are shown in (c) and (d). Hollow symbols in (a) and (b) represent the results of Monte Carlo simulations of 2D self-avoiding random walks on a square lattice. The level of confinement is $h/R_{ee} = 0.32$ for the chain length $N = 100$ and $h/R_{ee} = 0.12$ for $N = 500$. The solid lines in (a) and (b) represent equations (8). The size of the error bars is less than the symbols. The monomer index at which the radial fluctuations are equal to the perpendicular fluctuations $\chi^i_{xy} = \chi^i_z$ is obtained as $n^*/g = 4.8$.

remarking that the renormalized chain behaves as a two-dimensional (2D) chain composed of N/g blobs. Then the size of the chain is given as $\langle r_{xy}^2 \rangle^{1/2} \approx (N/g)^{\nu_2} h$, where $\nu_2 = 3/4$ is the Flory exponent for the 2D chain. By substitution, one can obtained the size of the chain in the x-y plane by $\langle r_{xy}^2 \rangle^{1/2} \approx N^{3/4} a \, (h/a)^{-1/4}$ (see Figure S1a). To go beyond scaling arguments, we remark that the system shares the main features of a self-avoiding walks (SAW) having n steps starting from origin and reaching point r_{xy}. In the limit $n \to \infty$ the asymptotic probability distribution reads[43,44]

$$P_n(r_{xy}) = \left(\frac{4}{R_n^{\alpha+1}} \right) \times r_{xy}^{\alpha} \times \exp\left[-(r_{xy}/R_n)^{\delta} \right], \tag{7}$$

with $\delta = 4$ for 2D SAW.[32] $R_n \approx h(n/g)^{3/4}$ is the Flory radius for 2D SAW with step size h and length normalized by blob size (g). By fitting equation 7 to $p_e(r_{xy})$ of a single chain of length $N = 100$, we found $\alpha = 1.4$ (Figure S4). Thus, the average position and fluctuations of different *fs* positioned at monomer index n_i are given by

$$\begin{aligned} \langle r_{xy}^i \rangle &= \int_0^{\infty} r_{xy} P_{n_i}(r_{xy}) dr_{xy} = \frac{\Gamma(\frac{\alpha+2}{4})}{\Gamma(\frac{\alpha+1}{4})} R_{n_i}, \\ \left(\chi_{xy}^i \right)^{1/2} &= \left[\frac{\Gamma(\frac{\alpha+3}{4})}{\Gamma(\frac{\alpha+1}{4})} - \left(\frac{\Gamma(\frac{\alpha+2}{4})}{\Gamma(\frac{\alpha+1}{4})} \right)^2 \right]^{1/2} R_{n_i} = A(\alpha) R_{n_i}, \end{aligned} \tag{8}$$

where Γ is the gamma function. Both size and fluctuations of the SAW scale with the Flory radius, $R_{n_i} \sim n_i^{3/4}$ and Eq. 8 collapses with the numerical results in Figure 3a and 3b. Additionally, we perform Monte Carlo (MC) simulation of self-avoiding walk on a 2D square lattice. The steps start from the origin, and the number of step are set by the number of blob, i.e., N/g. The average size and fluctuations of the steps with respect to the origin is shown in Figure 3a and b. The statistics is performed over 10^6 walks. Apart from the results of the initial steps, the results of 2D SAW reproduce well Molecular Dynamic (MD) results. The OP between different *fs* can be calculated by using the asymptotic probability distribution (Eq. 7) as shown in Figure 6 of SI.

The fluctuations of *fs* under confinement has two components: normal fluctuations which are set by the width of the slit $(\chi_z^i)^{1/2} \approx h/2$ and radial fluctuations $\left(\chi_{xy}^i\right)^{1/2}$ which are given by equation 8. In this regard, one can calculate the step number (monomer index) at which the fluctuations along radial direction are equal to the slit width. This becomes $n^* = g/A(\alpha)^{4/3}$. Given $\alpha = 1.4$ and blob size $g \approx 15$, which is set by the confinement level, the normalized crossing monomer index becomes $n^*/g \approx 5.1$, which is compatible to what is obtained from MD simulations $n^*/g \approx 4.8$ (Figure 3b). We also note that since in the blob picture each blob has k_BT energy, the confinement free energy can be obtained by $\Delta\mathcal{F}_c \approx (N/g)k_BT = N(h/a)^{-5/3}$ (see the Supplementary Information for more details). The confinement free energy of the chain $N = 100$ under confinement $h/R_{ee} = 0.32$, $\Delta\mathcal{F}_c = 18k_BT$ and average confining force $\langle F_z \rangle = 2.63k_BT/a$.

We observe in Figure 3c that the mean position increases with the monomer index with a 3/4 power scaling law. When the functional f is increased, the depletion zone close to the grafted region expands and the chain becomes more extended. The radial fluctuations of *fs* in Figure 3d also grows with monomer index while it is reduced by adding more functionals. In this case, the grafted patch resembles a star polymer under confinement. For a dilute solution of star polymers confined in a slit of width h, Halperin and Alexander[16] extended the Daoud-Cotton model[15] and proposed three different zones. (i) An interior region where the monomers behave as free star polymers of the effective blob size ξ and satisfying the conditions $r_{xy} < h$ and $\xi < h$. In this region, the monomers are concentrated and we expect the confinement does not affect the local structures. (ii) An intermediate zone where $r_{xy} > h$ and $\xi < h$. (iii) An exterior region $r_{xy} > h$ and $\xi > h$ where two-dimensional "superblobs" emerge. Because radial size of all *fs* is larger than the confinement level $\langle r_{xy}^i \rangle > h$ (Figure 3a), the *fs* are located either in the intermediate or exterior domain. The mean position of each *fs* of the confined star polymer in Figure 3c can be predicted by integrating the radial concentration of the monomers over radius of that *fs*, and compared with the total volume

of the star polymer of length n_i leading to[16]

$$\langle r_{xy}^i \rangle \sim f^{1/4} \left(\frac{a}{h}\right)^{1/4} n_i^{3/4} a, \tag{9}$$

The average radial position of the *fs* scales in an analogous way of a single grafted chain (see Figure 3c). The scaling of the average size of the chain with respect to the functionals f is checked in Figure 5 of SI. The position fluctuations in Figure 3d can be rationalized by equating the volume of the "super blobs" in the exterior region $\sim f\xi^2 h$ with the shell volume $\sim r_{xy}\xi h$ at radius r_{xy} yielding

$$\xi \sim \frac{\langle r_{xy}^i \rangle}{f} \sim f^{-3/4} \left(\frac{a}{h}\right)^{1/4} n_i^{3/4} a. \tag{10}$$

The scaling law $n_i^{3/4}$ is recovered in our simulation (Figure 3d) for large monomer index located in the exterior region. For smaller monomer index, we expect a deviation from scaling laws resulting from the finite size of the grafted region. As shown in the inset of Figures 3c and 3d, the position statistics of the end of chain $N = 100$ differ from the monomer of index $n = 100$ embedded within a chain $N = 500$: it is at a lower radius and fluctuated more.

The spatial ordering of the *fs* in the patch of chains originates also in the entropy reduction of the azimuthal degree of freedom, and we analyze its statistics. To do so, we increase the size patch f and compute in Figure 4 the azimuthal position statistics of the chain's end. The inset of Figure 4a shows the fluctuations of chain's end of four chains grafted at the corners of the 6×6 patch. Every end is localized not only radially but also azimuthally as a result of excluded volume between chains. The evolution of the azimuthal probability distribution with increasing *fs* is plotted in Figure 4a. For a single chain $f = 1$, the distribution is isotropic, and there is no preferred direction. In contrast, for a 3×3 patch ($f = 9$) the azimuthal distribution of one chain's end is peaked, and the maximum of likelihood is located at $\theta \simeq 0.6\pi$. The localization is even more pronounced for larger patches. We analyze

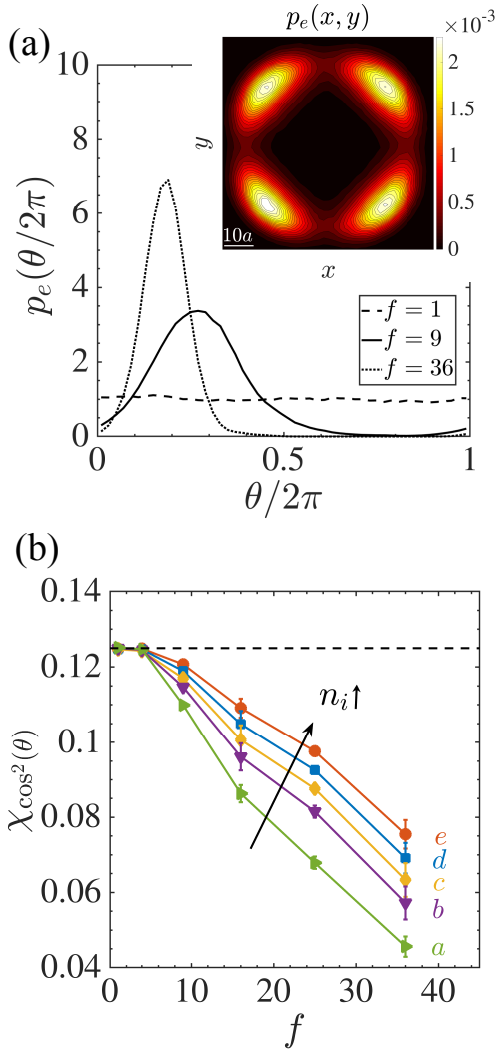

Figure 4: Azimuthal fluctuations. (a) Azimuthal probability distribution $p_e(\theta/2\pi)$ of one chain's end for a single chain (dashed) and inside a patch of size $f = 9$ (solid) and $f = 36$(dotted) under confinement. Inset shows the fluctuations of chain's end of four chains grafted at the corners of 6×6 patch. (b) Azimuthal fluctuations of fs ($\chi_{\cos^2(\theta)}$) as a function of functionals (f). The dashed line represents the azimuthal fluctuations of uniform distribution function, i.e., $p_e(\theta) = 1/2\pi$. The chain length is $N = 100$, and the confinement is $h/R_{ee} = 0.32$.

quantitatively in Figure 4b the azimuthal fluctuations $\chi_{\cos^2(\theta)}$ of the *fs* . We observe that the azimuthal fluctuations strongly reduce with the patch size and favor a localization of the *fs* . We expect this result to hold provided the patch size remains moderate and below the regime of polymer brush. Thus, by limiting the azimuthal fluctuations, a patch of chain shows a better spatial separation of *fs* than in a single-chain configuration.

Ordering Efficiency and Sequence Fidelity

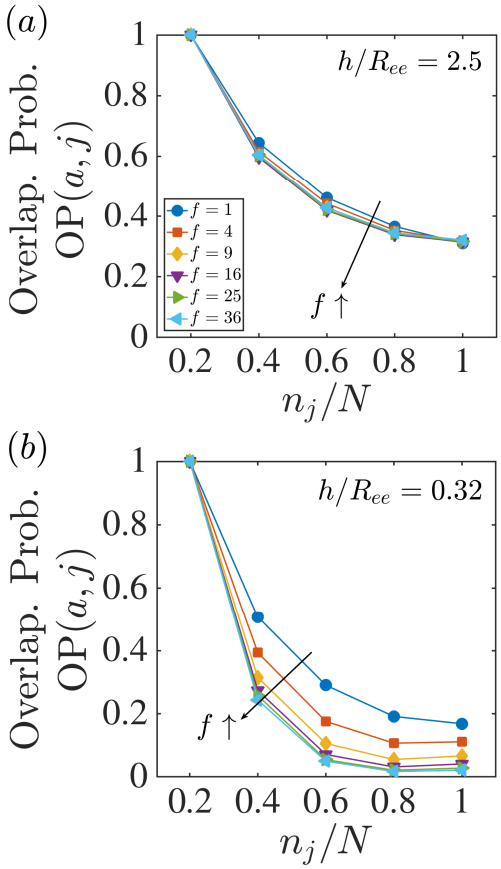

Figure 5: Overlapping probability (OP) between *fs* $\{a\}$ and other *fs* along the chain when the patch is free (a) and confined (b). The increase in the functionals f is marked with an arrow. The size of the chain is $N = 100$.

We summarize now the ordering properties and investigate the evolution of the Overlapping Probabilities (OPs) with confinement and patch size. In the unconfined situation, Figure 5 indicates that the OPs decrease with the distances between *fs* but remain large so

that no spatial order arises. Additionally in the unconfined situation the size of the patch does not play any major role provided the configuration remains smaller than a polymer brush. In contrast, in the confined state the OPs decrease strongly with monomer index. This trend is much more pronounced as the patch size increases and almost reaches zeros: for $f > 9$ the position of *fs* {a} weakly overlaps with *fs* {b} and does not overlap with *fs* {c}, {d}, and {e}. We observe an OP saturation limit for $f > 9$, above which the *fs* are almost completely localized away from the *fs* $\{a\}$. As the patch size is restrained to remain below the brush regime, we investigate the behavior of 3×3 patches of 4×4 grafted clusters with different intercluster distance (see Figure 9 in SI) but we observe no ordering enhancement.

Finally, we go beyond the spatial separation of two *fs* and calculate the probability of ordering spatially larger functional sequences P_{seq}. As shown in Figure 6a, we proceed by enumerating the events that the first three *fs* are sequenced radially, i.e., $r^a_{xy} < r^b_{xy} < r^c_{xy}$. Figure 6b shows that both confining and adding more functionals can largely enhance the sequencing ordering of *fs* even up to one for highly dense mushrooms. This can be explained by the excluded volume of the neighboring chains which prohibits the returning of the chains.

Conclusion

We investigate the ordering of the segments of grafted chains under planar confinement using molecular dynamics simulations and scaling laws. We show that confinement localizes the radial distribution of the segments and the localization is enhanced by adding more chain onto the grafted patch. We compute the averaged radial position and fluctuations of the segments. Both our results and asymptotic form of probability distribution of self-avoiding walks show that the radial fluctuations grow with Flory radius of the functional sites ($n_i^{3/4}$). We measure the overlapping probability between sites as a measure of the

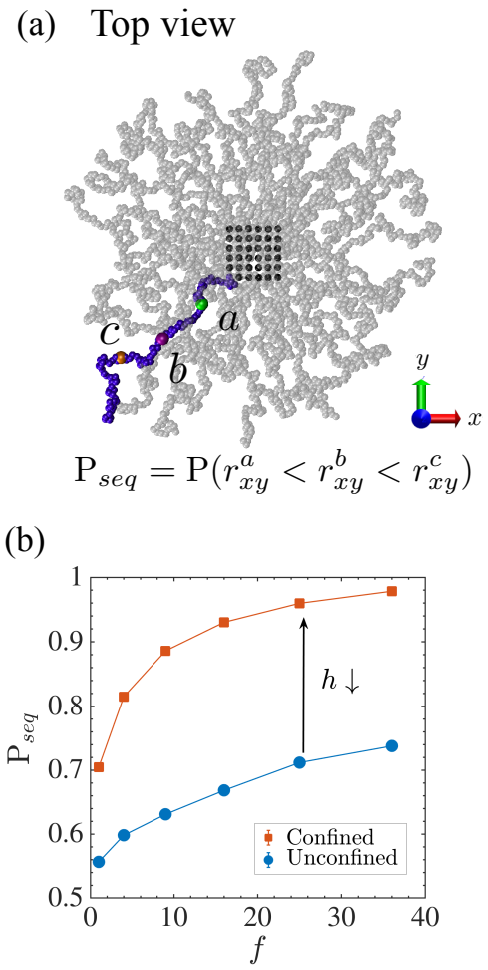

Figure 6: (a) Top view of a snapshot of system having $f = 36$ functionals. The sequencing probability of the first three *fs* is defined by $P_{seq} = P(r^a_{xy} < r^b_{xy} < r^c_{xy})$. (b) Probability of the sequencing ordering P_{seq} for chain length $N = 100$ as a function of functional f. The confining level is $h/R_{ee} = 0.32$.

ordering of the sites under confinement. The OP of single grafted chain decays with respect to the contour distance between the sites. By addition of more functionals, the OP can be further attenuated as the azimuthal fluctuations are diminished. Finally, confinement enhances the sequencing probability of the sites even close to one for a patch with large number of grafted chains. Thus, it is necessary to group chains into patches to increase the excluded volume effects. Making densely grafted homogeneous *brushes* is not a solution. Alternatively, absorbing star polymers or nanoparticles stabilized with grafted chains could lead to a similar effect as making patches of grafting chains. For biological systems our finding should be examined further by including specific interactions of functional groups with the backbone, with themselves and with surfaces.

Supporting Information

Detailed description of free energy calculation method and supporting figures.

References

(1) Lutz, J.-F.; Ouchi, M.; Liu, D. R.; Sawamoto, M. Sequence-controlled polymers. *Science* **2013**, *341*, 1238149.

(2) Bates, F.; Hillmyer, M.; Lodge, T.; Bates, C.; Delaney, K.; Fredrickson, G. Multiblock Polymers: Panacea or Pandora's Box? *Science* **2012**, *336*, 434–440.

(3) Kramer, J. W.; Treitler, D. S.; Dunn, E. W.; Castro, P. M.; Roisnel, T.; Thomas, C. M.; Coates, G. W. Polymerization of enantiopure monomers using syndiospecific catalysts: a new approach to sequence control in polymer synthesis. *Journal of the American Chemical Society* **2009**, *131*, 16042–16044.

(4) Ida, S.; Ouchi, M.; Sawamoto, M. Template-assisted selective radical addition toward

sequence-regulated polymerization: lariat capture of target monomer by template initiator. *Journal of the American Chemical Society* **2010**, *132*, 14748–14750.

(5) Ida, S.; Terashima, T.; Ouchi, M.; Sawamoto, M. Selective radical addition with a designed heterobifunctional halide: a primary study toward sequence-controlled polymerization upon template effect. *Journal of the American Chemical Society* **2009**, *131*, 10808–10809.

(6) McKee, M. L.; Milnes, P. J.; Bath, J.; Stulz, E.; Turberfield, A. J.; O'Reilly, R. K. Multistep DNA-templated reactions for the synthesis of functional sequence controlled oligomers. *Angewandte Chemie International Edition* **2010**, *49*, 7948–7951.

(7) Tong, X.; Guo, B.-h.; Huang, Y. Toward the synthesis of sequence-controlled vinyl copolymers. *Chemical Communications* **2011**, *47*, 1455–1457.

(8) Brudno, Y.; Liu, D. R. Recent progress toward the templated synthesis and directed evolution of sequence-defined synthetic polymers. *Chemistry & biology* **2009**, *16*, 265–276.

(9) Li, F.; Pincet, F.; Perez, E.; Eng, W. S.; Melia, T. J.; Rothman, J. E.; Tareste, D. Energetics and dynamics of SNAREpin folding across lipid bilayers. *Nature structural & molecular biology* **2007**, *14*, 890.

(10) Gruget, C.; Coleman, J.; Bello, O.; Krishnakumar, S. S.; Perez, E.; Rothman, J. E.; Pincet, F.; Donaldson Jr, S. H. Rearrangements under confinement lead to increased binding energy of Synaptotagmin-1 with anionic membranes in Mg2+ and Ca2+. *FEBS Letters* **2018**, *592*, 1497–1506.

(11) Cordier, P.; Tournilhac, F.; Soulié-Ziakovic, C.; Leibler, L. Self-healing and thermoreversible rubber from supramolecular assembly. *Nature* **2008**, *451*, 977.

(12) Chandra, P.; Jonas, A. M.; Fernandes, A. E. Sequence and Surface Confinement Direct Cooperativity in Catalytic Precision Oligomers. *Journal of the American Chemical Society* **2018**, *140*, 5179–5184.

(13) Curk, T.; Dobnikar, J.; Frenkel, D. Optimal multivalent targeting of membranes with many distinct receptors. *Proceedings of the National Academy of Sciences* **2017**, *114*, 7210–7215.

(14) Dubacheva, G. V.; Curk, T.; Mognetti, B. M.; Auzely-Velty, R.; Frenkel, D.; Richter, R. P. Superselective targeting using multivalent polymers. *Journal of the American Chemical Society* **2014**, *136*, 1722–1725.

(15) Daoud, M.; Cotton, J. Star shaped polymers : a model for the conformation and its concentration dependence. *Journal de Physique* **1982**, *43*, 531–538.

(16) Halperin, A.; Alexander, S. Confined star polymers. *Macromolecules* **1987**, *20*, 1146–1152.

(17) Odijk, T. The statistics and dynamics of confined or entangled stiff polymers. *Macromolecules* **1983**, *16*, 1340–1344.

(18) Benková, Z.; Námer, P.; Cifra, P. Comparison of a stripe and slab confinement for ring and linear macromolecules in nanochannel. *Soft Matter* **2016**, *12*, 8425–8439.

(19) Benková, Z.; Cifra, P. Simulation of semiflexible cyclic and linear chains moderatly and strongly confined in nanochannels. *Macromolecules* **2018**, *45*, 2597–2608.

(20) Chubak, I.; Locatelli, E.; Likos, C. Ring polymers are much stronger depleting agents than linear ones. *Molecular Physics* **2018**, *116*, 2911–2926.

(21) Li, F.; Pincet, F. Confinement Free Energy of Surfaces Bearing End-Grafted Polymers in the Mushroom Regime and Local Measurement of the Polymer Density. *Langmuir* **2007**, *23*, 12541–12548, PMID: 17988162.

(22) de Gennes, P.-G. Conformations of polymers attached to an interface. *Macromolecules* **1980**, *13*, 1069–1075.

(23) Paturej, J.; Milchev, A.; Egorov, S. A.; Binder, K. Star polymers confined in a nanoslit: a simulation test of scaling and self-consistent field theories. *Soft Matter* **2013**, *9*, 10522–10531.

(24) Likos, C.; Löwen, H.; Watzlawek, M.; Abbas, B.; Jucknischke, O.; Allgaier, J.; Richter, D. Star polymers viewed as ultrasoft colloidal particles. *Physical review letters* **1998**, *80*, 4450.

(25) Jusufi, A.; Watzlawek, M.; Löwen, H. Effective interaction between star polymers. *Macromolecules* **1999**, *32*, 4470–4473.

(26) Jusufi, A.; Dzubiella, J.; Likos, C.; Von Ferber, C.; Löwen, H. Effective interactions between star polymers and colloidal particles. *Journal of Physics: Condensed Matter* **2001**, *13*, 6177.

(27) Kremer, K.; Grest, G. S. Dynamics of entangled linear polymer melts: A molecular dynamics simulation. *The Journal of Chemical Physics* **1990**, *92*, 5057–5086.

(28) Plimpton, S. Fast parallel algorithms for short-range molecular dynamics. *Journal of computational physics* **1995**, *117*, 1–19.

(29) Dünweg, B.; Paul, W. Brownian dynamics simulations without Gaussian random numbers. *International Journal of Modern Physics C* **1991**, *02*, 817–827.

(30) Rouse, P. E. A Theory of the Linear Viscoelastic Properties of Dilute Solutions of Coiling Polymers. *The Journal of Chemical Physics* **1953**, *21*, 1272–1280.

(31) Doi, M. *Introduction to polymer physics*; Oxford university press, 1996.

(32) de Gennes, P.-G. *Scaling concepts in polymer physics*; Cornell university press, 1979.

(33) Doi, M.; Edwards, S. F. *The theory of polymer dynamics*; oxford university press, 1988; Vol. 73.

(34) Schneider, T.; Stoll, E. Molecular-dynamics study of a three-dimensional one-component model for distortive phase transitions. *Physical Review B* **1978**, *17*, 1302.

(35) Reith, D.; Milchev, A.; Virnau, P.; Binder, K. Computer simulation studies of chain dynamics in polymer brushes. *Macromolecules* **2012**, *45*, 4381–4393.

(36) Humphrey, W.; Dalke, A.; Schulten, K. VMD – Visual Molecular Dynamics. *Journal of Molecular Graphics* **1996**, *14*, 33–38.

(37) Rudnick, J.; Gaspari, G. The shapes of random walks. *Science* **1987**, *237*, 384–389.

(38) Haber, C.; Ruiz, S. A.; Wirtz, D. Shape anisotropy of a single random-walk polymer. *Proceedings of the National Academy of Sciences* **2000**, *97*, 10792–10795.

(39) Van Vliet, J.; Luyten, M.; Ten Brinke, G. Scaling behavior of dilute polymer solutions confined between parallel plates. *Macromolecules* **1992**, *25*, 3802–3806.

(40) Mazur, J.; Guttman, C. M.; McCrackin, F. L. Monte Carlo studies of self-interacting polymer chains with excluded volume. II. Shape of a chain. *Macromolecules* **1973**, *6*, 872–874.

(41) Daoud, M.; de Gennes, P.-G. Statistics of macromolecular solutions trapped in small pores. *Journal de physique* **1977**, *38*, 85–93.

(42) Sakaue, T.; Raphaël, E. Polymer chains in confined spaces and flow-injection problems: some remarks. *Macromolecules* **2006**, *39*, 2621–2628.

(43) Fisher, M. E. Shape of a Self-Avoiding Walk or Polymer Chain. *The Journal of Chemical Physics* **1966**, *44*, 616–622.

(44) Domb, C.; Gillis, J.; Wilmers, G. On the shape and configuration of polymer molecules. *Proceedings of the Physical Society* **1965**, *85*, 625.